

# Magnetic Field Created by Tile Permanent Magnets

R. Ravaud, G. Lemarquand, V. Lemarquand

## Abstract

This paper presents the analytical calculation of the three components of the magnetic field created by tile permanent magnets whose magnetization is either radial or axial. The calculations are based on the coulombian model of permanent magnets. The magnetic field is directly calculated, without the magnetic potential. Both axial and radial magnetization of the tiles are considered. The expressions obtained give the magnetic field in all the space. Such analytical expressions are very useful for the design and optimization of many industrial applications.

## Index Terms

Analytical model, magnetic field, permanent magnet, axial magnetization, radial magnetization

## I. INTRODUCTION

**A**FTER the parallelepiped, the most common shape for a permanent magnet in electrical engineering is certainly the tile, which can also be described as a ring sector. Such tiles can be either axially or radially magnetized. Therefore, the calculation of the magnetic field created by tile magnets is of great utility and numerous approaches exist.

Numerical approaches do not allow one to perform numerous parametric studies quickly and have generally a high computational cost. Consequently, authors are looking for alternative solutions. Their approaches are often semianalytical ones [1], and they represent important steps toward the ideal analytical

Manuscript Received April 10, 2008.

The authors are with the Laboratoire d'Acoustique de l'Universite du Maine UMR CNRS 6613, Avenue Olivier Messiaen, 72085 Le Mans Cedex 9, France

18 ones. In fact, different points of view can be adopted, which all look for the same thing: the calculation of  
19 the magnetic field and the magnetic forces. Kim et al. [2][3] calculate the magnetic force from the vector  
20 potential, with complete elliptic integrals and a mesh-matrix method. Kwon et al.[4] work with spherical  
21 coordinates and multipole expansions to calculate the far field of permanent magnet motors. Selvaggi et  
22 al.[5] propose an approach with cylindrical coordinates and the use of Green's function and Fourier series  
23 expansion to characterize the field from a set of permanent magnets. Babic and Akyel [6]-[8] calculate the  
24 force between coils thanks to Heuman's Lambda function. Toroidal harmonics yield interesting solutions  
25 to formulate the magnetic field created by permanent magnet cylinders [9]. Conway uses Bessel's function  
26 to calculate the inductance of coils using the vector potential [10] and proposes also a direct calculation  
27 of the magnetic field -without the vector potential- to reach the same goal [11].

28 While these studies show variety in the starting point for the problem they want to solve, many others  
29 are more specific and describe methods to calculate the magnetic field created by toroidal magnets. Perigo  
30 et al.[12] present analytical-integral expressions for the axial and radial magnetic flux density components  
31 of axially magnetized toroidal magnets, either on- or off-axis. The application considered is an electron  
32 beam focusing system. Zhilichev [13] works with cylindrical coordinates and uses separation of variables  
33 to evaluate the magnetic field from the scalar potential for tubular linear permanent magnet machines. He  
34 gives 2D and 3D approximations. Furlani et al. propose solutions based on the vector potential for radially  
35 polarized multipole cylindrical magnets [14] as well as for axially polarized magnets for axial field motors  
36 [15][16]. Rakotoarison et al.[17] give a semianalytical method to calculate the field created by radially  
37 magnetized tile magnets from the scalar potential. They use a coulombian model of the magnets and take  
38 the volume charge density into account.

39 All the studies dedicated to the calculation of the magnetic field created by toroidal or tile magnets are  
40 very useful: they constitute tools for the design and the optimization of devices which use such magnets  
41 and enable to meet specific requirements. For example, tile magnets with rotating magnetizations are  
42 used to make discrete Halbach cylinders [18] which have various applications, such as electrodynamic  
43 wheels [19] for maglev devices, the creation of homogeneous fields or tailored gradient fields [20], the  
44 magnetization of brushless machines to obtain sinusoidal field variation in the airgap [21]. Tile magnets  
45 are used with peculiar profiles to reduce the cogging torque in axial flux machines [22] as well as in radial

46 flux ones [23], but also to control the torque in permanent magnet couplings [24][25] and gears. They  
 47 are constitutive parts of displacement sensors [26] and also ironless loudspeakers [27][28] demonstrating  
 48 their widespread use.

49 This paper presents analytical expressions for the three components of the magnetic field created by  
 50 tile permanent magnets. The magnetic field is directly calculated, without a previous calculation of the  
 51 scalar or vector potential[29][30][31]. The expressions given are for a ring sector, but remain valid when  
 52 the sector is extended to the whole ring. The axial magnetization of the tiles is considered in the first  
 53 section below and the radial magnetization in the second.

## 54 II. AXIALLY MAGNETIZED TILES

### 55 A. Notation and Geometry

56 The geometry which is considered is a tile permanent magnet and the related parameters are shown  
 57 in Fig.1. The tile inner radius is  $r_{in}$ , the tile outer one is  $r_{out}$  and its height is  $h$ . The angular width of  
 58 the tile is  $\theta_2 - \theta_1$ . The axis  $z$  is an axis of symmetry. The coulombian model of a permanent magnet is  
 59 used. Consequently, the tile permanent magnet is represented by two curved planes which correspond to  
 60 the upper ( $z = h$ ) and lower ( $z = 0$ ) faces of the ring sector. The upper one is charged with a surface  
 61 magnetic pole density  $+\sigma^*$ ; the lower one is charged with the opposite surface magnetic pole density  
 62  $-\sigma^*$ . All the illustrative calculations are done with  $\sigma^* = \vec{J} \cdot \vec{n} = 1T$ . In order to simplify the calculations,  
 63 the upper face only is taken into account to determine the three magnetic field components. However,  
 64 the total magnetic field can be calculated by the application of the linear superposition principle to both  
 65 faces.

66 Let us consider a point  $P$  on the ring sector upper face. The magnetic field  $\vec{H}$  created by the source  
 67 point  $P(r, \theta_s, z)$  at any observation point  $M(r, \theta, z)$  of the space is given by (1).

$$\vec{H}(r, \theta, z) = \frac{\sigma^*}{4\pi\mu_0} \int_{\theta_1}^{\theta_2} \int_{r_{in}}^{r_{out}} \frac{\overrightarrow{PM}}{|\overrightarrow{PM}|^3} r_1 dr_1 d\theta_s \quad (1)$$

68 where  $\mu_0$  is the vacuum magnetic permeability ( $\mu_0 = 4\pi \cdot 10^{-7} SI$ ) and  $\sigma^*$  is the fictitious magnetic pole

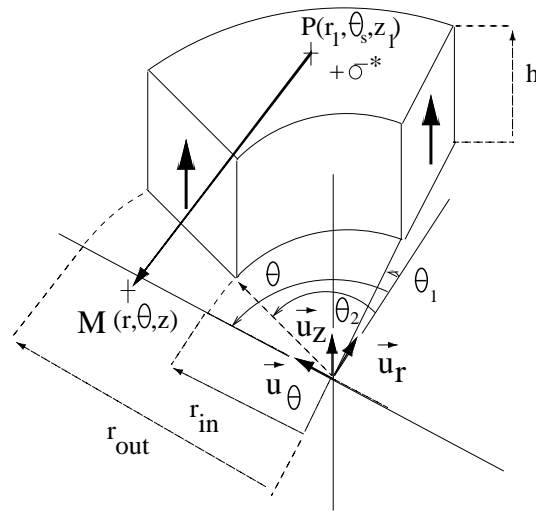


Fig. 1. Axially magnetized tile permanent magnet : parameter definition.

69 surface density in tesla. Equation (1) can be written as follows:

$$\vec{H}(r, \theta, z) = \frac{\sigma^*}{4\pi\mu_0} \int_{\theta_1}^{\theta_2} \int_{r_{in}}^{r_{out}} \frac{(r - r_1 \cos(\theta - \theta_s))\vec{u}_r - r_1 \sin(\theta_s - \theta)\vec{u}_\theta + (z - z_1)\vec{u}_z}{(r_1^2 + r^2 + (z - z_1)^2 - 2r_1 r \cos(\theta - \theta_s))^{\frac{3}{2}}} r_1 dr_1 d\theta_s \quad (2)$$

70 B. Components along the three directions  $\vec{u}_r$ ,  $\vec{u}_\theta$ ,  $\vec{u}_z$

71 The integration of (2) leads to the magnetic field components along the three axes defined  $H_r(r, \theta, z)$ ,  
72  $H_\theta(r, \theta, z)$ ,  $H_z(r, \theta, z)$ .

73 1) Azimuthal component  $H_\theta(r, \theta, z)$ : The magnetic field azimuthal component  $H_\theta(r, \theta, z)$  created by  
74 the upper face is given by (3).

$$H_\theta(r, \theta, z) = \frac{\sigma^*}{4\pi\mu_0} (\eta(\theta, \theta_1) - \eta(\theta, \theta_2)) \quad (3)$$

75 with

$$\begin{aligned} \eta(\theta, \theta_i) = & \frac{\sqrt{r^2 + r_{in}^2 + (z - h)^2 - 2rr_{in} \cos(\theta_i - \theta)}}{r} \\ & + \cos(\theta_i - \theta) \log \left[ r_{in} - r \cos(\theta_i - \theta) + \sqrt{r^2 + r_{in}^2 + (z - h)^2 - 2rr_{in} \cos(\theta_i - \theta)} \right] \\ & - \frac{\sqrt{r^2 + r_{out}^2 + (z - h)^2 - 2rr_{out} \cos(\theta_i - \theta)}}{r} \end{aligned}$$

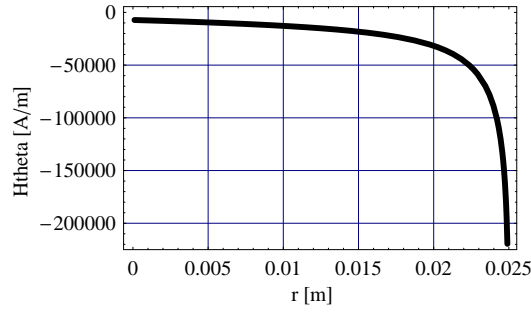


Fig. 2. Field azimuthal component  $H_\theta(r, \theta, z)$  versus the radial distance  $r$  of the observation point;  $h = 3\text{mm}$ ,  $r_{in} = 25\text{mm}$ ,  $r_{out} = 28\text{mm}$ ,  $\theta_1 = 0$ ,  $\theta_2 = \frac{\pi}{2}$ ,  $\theta = \frac{\pi}{2}$

$$-\cos(\theta_i - \theta) \log \left[ r_{out} - r \cos(\theta_i - \theta) + \sqrt{r^2 + r_{out}^2 + (z - h)^2 - 2rr_{out} \cos(\theta_i - \theta)} \right] \quad (4)$$

76 Equation (3) is valid for any observation point  $M(r, \theta, z)$  with  $0 \leq \theta \leq 2\pi$ . Figure 2 represents the  
 77 azimuthal component  $H_\theta(r, \theta, z)$  versus the radial distance  $r$  of the observation point. The parameter values  
 78 are  $h = 3\text{ mm}$ ,  $\theta_1 = 0\text{ rad}$ ,  $\theta_2 = \frac{\pi}{2}\text{ rad}$ ,  $\theta = 0\text{ rad}$ ,  $r_{in} = 25\text{ mm}$ ,  $r_{out} = 28\text{ mm}$ .

79 2) *Radial component  $H_r(r, \theta, z)$* : The field radial component  $H_r(r, \theta, z)$  created by the upper face is  
 80 given by (5).

$$H_r(r, \theta, z) = \frac{\sigma^*}{4\pi\mu_0} (\alpha(u_2, r, z) - \alpha(u_1, r, z)) \quad (5)$$

81 where

$$u_i = \cos(\theta - \theta_i) \quad (6)$$

82 and

$$\begin{aligned} \alpha(u_i, r, z) = & F_1(u_i, r, z) \left( G_1(u_i, r, z) \mathbf{E}^* \left[ \arcsin \left[ \frac{\sqrt{r^2 + r_{out}^2 - 2rr_{out}u_i + (z-h)^2}}{(r+r_{out})^2 + (z-h)^2} \right], \frac{(r+r_{out})^2 + (z-h)^2}{(r-r_{out})^2 + (z-h)^2} \right] \right) \\ & + F_1(u_i, r, z) \Pi^* \left[ \arcsin \left[ \frac{\sqrt{r^2 + r_{out}^2 - 2rr_{out}u_i + (z-h)^2}}{(r+r_{out})^2 + (z-h)^2} \right], \frac{(r+r_{out})^2 + (z-h)^2}{(r-r_{out})^2 + (z-h)^2} \right] \\ & - F_2(u_i, r, z) \left( G_2(u_i, r, z) \mathbf{E}^* \left[ \arcsin \left[ \frac{\sqrt{r^2 + r_{in}^2 - 2rr_{in}u_i + (z-h)^2}}{(r+r_{in})^2 + (z-h)^2} \right], \frac{(r+r_{in})^2 + (z-h)^2}{(r-r_{in})^2 + (z-h)^2} \right] \right) \end{aligned}$$

$$\begin{aligned}
& -F_2(u_i, r, z)\Pi^* \left[ \arcsin\left[\frac{\sqrt{r^2 + r_{in}^2 - 2rr_{in}u_i + (z-h)^2}}{(r+r_{in})^2 + (z-h)^2}\right], \frac{(r+r_{in})^2 + (z-h)^2}{(r-r_{in})^2 + (z-h)^2} \right] \\
& + \frac{(u_i^2 - 1)}{\sqrt{1 - u_i^2}} \log \left[ r_{out} - ru_i + \sqrt{r^2 + r_{out}^2 - 2rr_{out}u_i + (z-h)^2} \right] \\
& - \frac{(u_i^2 - 1)}{\sqrt{1 - u_i^2}} \log \left[ r_{in} - ru_i + \sqrt{r^2 + r_{in}^2 - 2rr_{in}u_i + (z-h)^2} \right]
\end{aligned} \tag{7}$$

83 with :

$$F_1(u_i, r, z) = \frac{1}{\sqrt{1 - u_i^2}} \frac{2r_{out}(1 + u_i) \sqrt{\frac{rr_{out}(u_i-1)}{(r-r_{out})^2 + (z-h)^2}} \sqrt{\frac{r^2 + r_{out}^2 - 2rr_{out}u_i + (z-h)^2}{(r+r_{out})^2 + (z-h)^2}}}{\sqrt{\frac{rr_{out}(1+u_i)}{(r+r_{out})^2 + (z-h)^2}} \sqrt{r^2 + r_{out}^2 - 2rr_{out}u_i + (z-h)^2}} \tag{8}$$

84

$$F_2(u_i, r, z) = \frac{1}{\sqrt{1 - u_i^2}} \frac{2r_{in}(1 + u_i) \sqrt{\frac{rr_{in}(u_i-1)}{(r-r_{in})^2 + (z-h)^2}} \sqrt{\frac{r^2 + r_{in}^2 - 2rr_{in}u_i + (z-h)^2}{(r+r_{in})^2 + (z-h)^2}}}{\sqrt{\frac{rr_{in}(1+u_i)}{(r+r_{in})^2 + (z-h)^2}} \sqrt{r^2 + r_{in}^2 - 2rr_{in}u_i + (z-h)^2}} \tag{9}$$

85

$$G_1(r, z) = \frac{(r - r_{in})^2 + (z - h)^2}{2rr_{in}} \tag{10}$$

86

$$G_2(r, z) = \frac{(r - r_{out})^2 + (z - h)^2}{2rr_{out}} \tag{11}$$

87

$$E^*[k] = \int_0^{\phi=\frac{\pi}{2}} \sqrt{1 - k^2 \sin^2(\theta)} d\theta \tag{12}$$

88 Equation (5) is valid for any observation point  $M(r, \theta, z)$  with  $\theta \neq \theta_i$  and  $0 \leq \theta < 2\pi$ . This expression  
89 remains valid for ring permanent magnets, for which the angular width is  $2\pi$  ( $\theta_2 - \theta_1 = 2\pi$ ). It leads  
90 to the expression of the radial component already given by the authors for ring magnets [32]. Figure 3  
91 represents the field radial component  $H_r(r, \theta, z)$  versus the radial distance  $r$ . The used parameters are  
92  $h = 3$  mm,  $\theta_1 = 0$  rad,  $\theta_2 = \frac{\pi}{2}$  rad,  $\theta = 0$  rad,  $r_{in} = 25$  mm,  $r_{out} = 28$  mm.

93 3) Axial component  $H_z(r, \theta, z)$ : The field axial component  $H_z(r, \theta, z)$  created by the upper face is  
94 given by (13).

$$H_z(r, \theta, z) = \frac{\sigma^*}{4\pi\mu_0} (\gamma(\theta, \theta_2) - \gamma(\theta, \theta_1)) \tag{13}$$

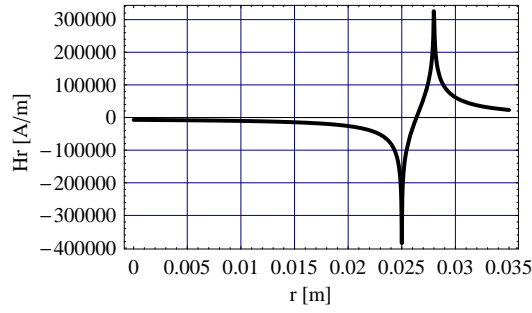


Fig. 3. Field radial component  $H_r(r, \theta, z)$  versus the radial distance  $r$  of the observation point;  $h = 3\text{mm}$ ,  $r_{in} = 25\text{mm}$ ,  $r_{out} = 28\text{mm}$ ,  $\theta_1 = 0\text{ rad}$ ,  $\theta_2 = \frac{\pi}{2}\text{ rad}$ ,  $\theta = \frac{\pi}{2}\text{ rad}$

95 with

$$\begin{aligned}
 \gamma(\theta, \theta_i) = & h_1 \eta_1(\theta, \theta_i) \mathbf{\Pi}^* \left[ \frac{2(c_1 + d_1)f}{2c_1f - \sqrt{2}\sqrt{d_1^2 f(-e + f)}}, i \sinh^{-1} \left[ \sqrt{\frac{-1}{c_1 + d_1}} \sqrt{c_1 - d_1 \cos(\theta - \theta_i)} \right], \frac{c_1 + d_1}{c_1 - d_1} \right] \\
 & + h_2 \eta_1(\theta, \theta_i) \mathbf{\Pi}^* \left[ \frac{2(c_1 + d_1)f}{2c_1f + \sqrt{2}\sqrt{d_1^2 f(-e + f)}}, i \sinh^{-1} \left[ \sqrt{\frac{-1}{c_1 + d_1}} \sqrt{c_1 - d_1 \cos(\theta - \theta_i)} \right], \frac{c_1 + d_1}{c_1 - d_1} \right] \\
 & - h_3 \eta_2(\theta, \theta_i) \mathbf{\Pi}^* \left[ \frac{2(c_2 + d_2)f}{2c_2f - \sqrt{2}\sqrt{d_2^2 f(-e + f)}}, i \sinh^{-1} \left[ \sqrt{\frac{-1}{c_2 + d_2}} \sqrt{c_2 - d_2 \cos(\theta - \theta_i)} \right], \frac{c_2 + d_2}{c_2 - d_2} \right] \\
 & - h_4 \eta_2(\theta, \theta_i) \mathbf{\Pi}^* \left[ \frac{2(c_2 + d_2)f}{2c_2f + \sqrt{2}\sqrt{d_2^2 f(-e + f)}}, i \sinh^{-1} \left[ \sqrt{\frac{-1}{c_2 + d_2}} \sqrt{c_2 - d_2 \cos(\theta - \theta_i)} \right], \frac{c_2 + d_2}{c_2 - d_2} \right]
 \end{aligned} \tag{14}$$

96 with

$$\eta_1(\theta, \theta_i) = \frac{\left( -i \sqrt{\frac{d_1(-1 + \cos(\theta - \theta_i))}{c_1 - d_1}} \sqrt{\frac{d_1(1 + \cos(\theta - \theta_i))}{c_1 + d_1}} \frac{1}{\cos(\theta - \theta_i)} \right)}{\left( 2 \sqrt{\frac{-1}{c_1 + d_1}} \sqrt{d_1^2 f(-e + d_1)} (d_1^2 (e - f)) + 2c_1^2 f \right)} \tag{15}$$

97

$$\eta_2(\theta, \theta_i) = \frac{\left( -i \sqrt{\frac{d_2(-1 + \cos(\theta - \theta_i))}{c_2 - d_2}} \sqrt{\frac{d_2(1 + \cos(\theta - \theta_i))}{c_2 + d_2}} \frac{1}{\cos(\theta - \theta_i)} \right)}{\left( 2 \sqrt{\frac{-1}{c_2 + d_2}} \sqrt{d_2^2 f(-e + d_2)} (d_2^2 (e - f)) + 2c_2^2 f \right)} \tag{16}$$

98

$$h_1 = 2ad_1(\sqrt{2}c_1f + \sqrt{d_1^2 f(-e + f)}) + b_1(\sqrt{2}d_1^2(e - f) - 2c_1\sqrt{d_1^2 f(-e + f)}) \tag{17}$$

Parameters	
$a$	$2(z-h)(r^2+(z-h)^2)$
$b_1$	$2(z-h)rr_{out}$
$c_1$	$r^2+r_{out}^2+(z-h)^2$
$d_1$	$-2rr_{out}$
$e$	$-r^2-2(z-h)^2$
$f$	$r^2$
$b_2$	$2(z-h)rr_{in}$
$c_2$	$r^2+r_{in}^2+(z-h)^2$
$d_2$	$-2rr_{in}$

TABLE I  
DEFINITION OF THE PARAMETERS USED IN (13)

$$h_2 = 2ad_1(-\sqrt{2}c_1f + \sqrt{d_1^2f(-e+f)}) + b_1(\sqrt{2}d_1^2(-e+f) - 2c_1\sqrt{d_1^2f(-e+f)}) \quad (18)$$

$$h_3 = 2ad_2(\sqrt{2}c_2f + \sqrt{d_2^2f(-e+f)}) + b_2(\sqrt{2}d_2^2(e-f) - 2c_2\sqrt{d_2^2f(-e+f)}) \quad (19)$$

$$h_4 = 2ad_2(-\sqrt{2}c_2f + \sqrt{d_2^2f(-e+f)}) + b_2(\sqrt{2}d_2^2(-e+f) - 2c_2\sqrt{d_2^2f(-e+f)}) \quad (20)$$

where  $\Pi^*[n, \phi, m]$  is given in terms of the incomplete elliptic integral of the third kind by (21).

$$\Pi^*[n, \phi, m] = \int_0^\phi \frac{1}{(1-n\sin(\theta)^2)\sqrt{1-m\sin(\theta)^2}} d\theta \quad (21)$$

Although the result  $H_z(r, \theta, z)$  is a real number, equation (14) contains the imaginary number  $i$  ( $i^2 = -1$ ) because we did not succeed in obtaining a real expression for the axial component  $H_z(r, \theta, z)$ . The parameters used in (14) are defined in Table I. However, as the imaginary part is the consequence of numerical noise and nearly equals zero, when the expression (14) is used in symbolic mathematical tools such as Mathematica or Maple, the real part of  $H_z(r, \theta, z)$  only has to be considered. Equation (13) is valid for any observation point  $M(r, \theta, z)$  with  $\theta \neq \theta_i$  and  $0 \leq \theta < 2\pi$ . Here again, this expression remains valid for ring permanent magnets, i.e. when the angular width is  $2\pi$  ( $\theta_2 - \theta_1 = 2\pi$ ). It also leads to the expression of the axial component already given by the authors for ring magnets [32]. Figure 4 represents the axial component  $H_z(r, \theta, z)$  versus the radial distance  $r$  of the observation point. The parameter values are  $h = 3$  mm,  $\theta_1 = 0$  rad,  $\theta_2 = \frac{\pi}{2}$  rad,  $\theta = 0$  rad,  $r_{in} = 25$  mm,  $r_{out} = 28$  mm.

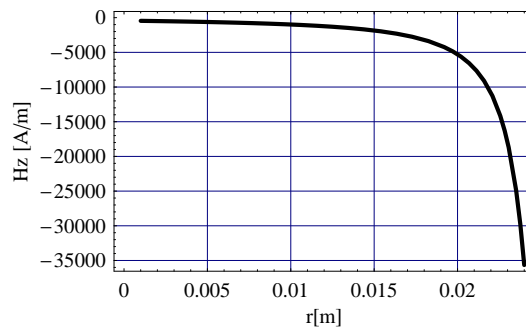


Fig. 4. Field axial component  $H_z(r, \theta, z)$  versus the radial distance  $r$  of the observation point;  $h = 3mm$ ,  $r_{in} = 25mm$ ,  $r_{out} = 28mm$ ,  $\theta_1 = 0$  rad,  $\theta_2 = \frac{\pi}{2}$  rad,  $\theta = \frac{\pi}{2}$  rad

### III. RADIALY MAGNETIZED TILES

113

#### A. Notation and geometry

114

115 The geometry and its parameters are shown in Fig.(5). The axis  $z$  is an axis of symmetry. Again, the  
 116 coulombian model of permanent magnets is used. The permanent magnet ring sector is thus represented  
 117 by two curved planes which correspond here to the inner and outer faces of the ring. The inner face is  
 118 charged with a magnetic pole surface density  $+\sigma^*$ ; the outer one is charged with the opposite magnetic  
 119 pole surface density  $-\sigma^*$ . We only consider the inner face to simplify the analytical calculation. As stated  
 120 previously, the total magnetic field can be calculated by the application of the linear superposition principle  
 121 to both faces.

122 The magnetic pole volume density is not taken into account in this paper. This means that the total sum  
 123 of all the charges in the model does not equal zero. Indeed, as the magnetization is radial, the magnetic  
 124 pole surface density of the curved planes is uniform. The charge on the outer plane is thus greater than  
 125 the charge on the inner plane, as the surfaces of these planes. The volume charge density, linked to the  
 126 magnetization divergence, appears in fact to set the global charge to zero. If the radial width of the tile is  
 127 small, which also means that the tile is thin, then the difference between the inner and outer plane surface  
 128 is small, and so is the magnetic pole volume density: its neglecting is an acceptable approximation. This  
 129 approximation becomes less and less valid when the thickness of the tile increases. This paper presents  
 130 expressions for radially magnetized thin tiles.

131 Let us consider a point  $P$  on the tile inner face. The magnetic field  $\vec{H}$  created by the source point

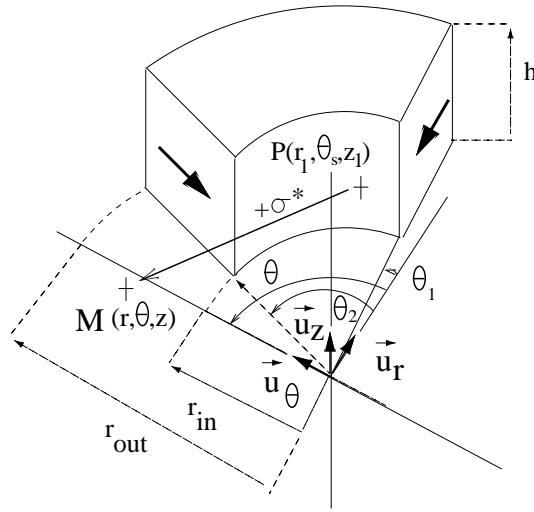


Fig. 5. Radially magnetized permanent magnet tile: parameter definition

132  $P(r, \theta_s, z)$  at any observation point  $M(r, \theta, z)$  of the space is given by (22).

$$\vec{H}(r, \theta, z) = \frac{\sigma^*}{4\pi\mu_0} \int_{\theta_1}^{\theta_2} \int_0^h \frac{\overline{PM}}{|\overline{PM}|^3} r_1 dz_1 d\theta_s \quad (22)$$

133 where  $\mu_0$  is the magnetic permeability of the vacuum ( $\mu_0 = 4\pi \cdot 10^{-7} SI$ ) and  $\sigma^*$  is the fictitious magnetic  
134 pole surface density given in tesla . Equation (22) can be written as follows:

$$\vec{H}(r, \theta, z) = \frac{\sigma^*}{4\pi\mu_0} \int_{\theta_1}^{\theta_2} \int_0^h \frac{(r - r_1 \cos(\theta - \theta_s))\vec{u}_r - r_1 \sin(\theta_s - \theta)\vec{u}_\theta + (z - z_1)\vec{u}_z}{(r_1^2 + r^2 + (z - z_1)^2 - 2r_1 r \cos(\theta - \theta_s))^{\frac{3}{2}}} r_1 dz_1 d\theta_s \quad (23)$$

135 **B. Components along the three directions  $\vec{u}_r$ ,  $\vec{u}_\theta$ ,  $\vec{u}_z$**

136 The integration of (23) leads to the magnetic field components created by the inner face along the three  
137 axes defined  $H_r(r, \theta, z)$ ,  $H_\theta(r, \theta, z)$ ,  $H_z(r, \theta, z)$ .

138 1) *Azimuthal component  $H_\theta(r, \theta, z)$* : The field azimuthal component  $H_\theta(r, \theta, z)$  is given by (24).

$$H_\theta(r, \theta, z) = \frac{\sigma}{4\pi\mu_0} (\beta(\theta, \theta_1) - \beta(\theta, \theta_2)) \quad (24)$$

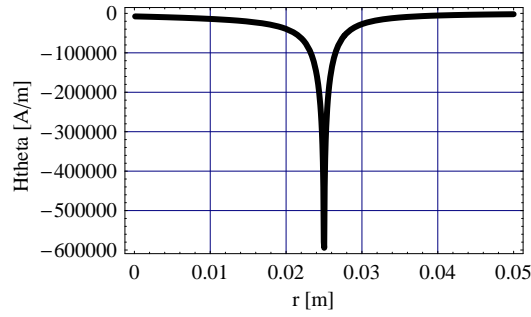


Fig. 6. Field azimuthal component  $H_\theta(r, \theta, z)$  versus the radial distance  $r$  of the observation point;  $h = 3$  mm,  $r_{in} = 25$  mm,  $r_{out} = 28$  mm,  $\theta_1 = 0$  rad,  $\theta_2 = \frac{\pi}{2}$  rad,  $\theta = 0$  rad

139 with

$$\beta(\theta, \theta_i) = \frac{r_{in}(b-z)}{r\sqrt{-(b-z)^2}} \arctan \left[ \frac{\sqrt{r^2 + r_{in}^2 + (b-z)^2 - 2rr_{in} \cos(\theta_i - \theta)}}{\sqrt{-(b-z)^2}} \right] - \frac{r_{in}}{r} \tanh^{-1} \left[ \frac{\sqrt{r^2 + r_{in}^2 + z^2 - 2rr_{in} \cos(\theta_i - \theta)}}{z} \right] \quad (25)$$

140 Equation (24) is valid for any observation point  $M(r, \theta, z)$  with  $0 \leq \theta \leq 2\pi$ . Figure 6 represents the  
 141 azimuthal component  $H_\theta(r, \theta, z)$  versus the radial distance  $r$  of the observation point. The parameters  
 142 values are  $h = 3$  mm,  $\theta_1 = 0$ ,  $\theta_2 = \frac{\pi}{2}$ ,  $\theta = 0$ ,  $r_{in} = 25$  mm,  $r_{out} = 28$  mm.

143 2) Radial component  $H_r(r, \theta, z)$ : The radial component of the field  $H_r(r, \theta, z)$  is given by (26).

$$H_r(r, \theta, z) = \frac{\sigma^*}{4\pi\mu_0} (\beta(u_1) - \beta(u_2)) \quad (26)$$

144 with

$$u_i = \cos(\theta - \theta_i) \quad (27)$$

145 and

$$\beta(u_i) = \left( \frac{2i(1+u_i)\sqrt{\frac{d(-1+u_i)}{c+e_1+du_i}}(-a_1d+b_1(c+e_1))\mathbf{F}^* \left[ i \sinh^{-1} \left[ \frac{\sqrt{-c+d-e_1}}{\sqrt{c+e_1+du_i}}, \frac{c+d+e_1}{c-d+e_1} \right] \right]}{d\sqrt{-c+d-e_1}e_1\sqrt{\frac{d(1+u_i)}{c+e_1+du_i}}\sqrt{1-u_i^2}} \right)$$

Parameters	
$a_1$	$r_{in} r z$
$b_1$	$-r_{in}^2 z$
$c$	$r^2 + r_{in}^2$
$d$	$-2r r_{in}$
$e_1$	$z^2$
$a_2$	$-r_{in} r (z - h)$
$b_2$	$r_{in}^2 (z - h)$
$e_2$	$(z - h)^2$

TABLE II  
DEFINITION OF THE PARAMETERS USED IN (26)

$$\begin{aligned}
& + \left( \frac{2i(1+u_i) \sqrt{\frac{d(-1+u_i)}{c+e_1+du_i}} (b_1 c - a_1 d) \mathbf{\Pi}^* \left[ \frac{e_1}{c-d+e_1}, i \sinh^{-1} \left[ \frac{\sqrt{-c+d+e_1}}{c+e_1+du_i} \right], \frac{c+d+e_1}{c-d+e_1} \right]}{d \sqrt{-c+d-e_1} e_1 \sqrt{\frac{d(1+u_i)}{c+e_1+du_i}} \sqrt{1-u_i^2}} \right) \\
& + \left( \frac{2i(1+u_i) \sqrt{\frac{d(-1+u_i)}{c+e_2+du_i}} (-a_2 d + b_2 (c+e_2)) \mathbf{F}^* \left[ i \sinh^{-1} \left[ \frac{\sqrt{-c+d-e_2}}{\sqrt{c+e_2+du_i}} \right], \frac{c+d+e_2}{c-d+e_2} \right]}{d \sqrt{-c+d-e_2} e_2 \sqrt{\frac{d(1+u_i)}{c+e_2+du_i}} \sqrt{1-u_i^2}} \right) \\
& + \left( \frac{2i(1+u_i) \sqrt{\frac{d(-1+u_i)}{c+e_2+du_i}} (b_2 c - a_2 d) \mathbf{\Pi}^* \left[ \frac{e_2}{c-d+e_2}, i \sinh^{-1} \left[ \frac{\sqrt{-c+d+e_2}}{c+e_2+du_i} \right], \frac{c+d+e_2}{c-d+e_2} \right]}{d \sqrt{-c+d-e_2} e_2 \sqrt{\frac{d(1+u_i)}{c+e_2+du_i}} \sqrt{1-u_i^2}} \right)
\end{aligned} \tag{28}$$

146 where  $F^*[\phi, m]$  is defined by (31) and  $\mathbf{\Pi}^*[n, \phi, m]$  is given by (21). Here again, Eq.(28) contains the  
147 imaginary number  $i$  ( $i^2 = -1$ ) although the result  $H_r(r, z)$  is a real number because we did not succeed in  
148 obtaining a real expression for the radial component  $H_r(r, \theta, z)$ . The parameters used in (28) are defined  
149 in Table II. Of course, when using the expression (28) in tools like Mathematica or Mapple, the imaginary  
150 part of  $H_r(r, \theta, z)$  has to be dropped, as it only corresponds to numerical noise and nearly equals zero.

151 Equation (26) can be used to calculate the radial component of the magnetic field at any observation  
152 point  $M(r, \theta, z)$  with  $\theta \neq \theta_i$  and  $0 \leq \theta < 2\pi$ . When the tile angular width becomes  $2\pi$  ( $\theta_2 - \theta_1 = 2\pi$ ),  
153 so for ring magnets, the expression becomes the one already given in a previous paper [32]. Figure 7  
154 represents the field radial component  $H_r(r, \theta, z)$  versus the radial distance  $r$  of the observation point. The  
155 parameter values are  $h = 3$  mm,  $\theta_1 = 0$  rad,  $\theta_2 = \frac{\pi}{2}$  rad,  $\theta = 0$  rad,  $r_{in} = 25$  mm,  $r_{out} = 28$  mm.

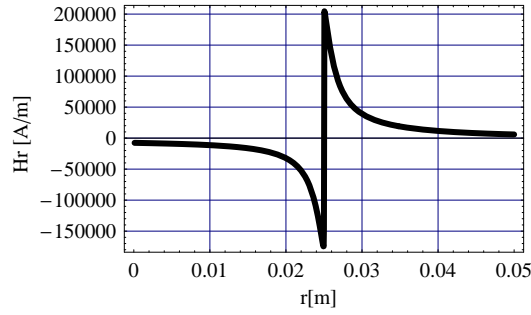


Fig. 7. Field radial component  $H_r(r, \theta, z)$  versus the radial distance  $r$  of the observation point;  $h = 3$  mm,  $r_{in} = 25$  mm,  $r_{out} = 28$  mm,  $\theta_1 = 0$  rad,  $\theta_2 = \frac{\pi}{2}$  rad,  $\theta = \frac{\pi}{2}$  rad

156 3) Axial component  $H_z(r, \theta, z)$  : The field axial component  $H_z(r, \theta, z)$  is given by (29):

$$H_z(r, \theta, z) = \frac{\sigma^*}{4\pi\mu_0} (\alpha(\theta, \theta_2) - \alpha(\theta, \theta_1)) \quad (29)$$

157 with

$$\alpha(\theta, \theta_i) = \frac{2r_{in}}{(r - r_{in})^2 + (z - h)^2} \mathbf{F}^* \left[ \frac{\theta - \theta_i}{2}, -\frac{4rr_{in}}{(r - r_{in})^2 + (z - h)^2} \right] - \frac{2r_{in}}{(r - r_{in})^2 + z^2} \mathbf{F}^* \left[ \frac{\theta - \theta_i}{2}, -\frac{4rr_{in}}{(r - r_{in})^2 + z^2} \right] \quad (30)$$

158 where  $\mathbf{F}^*[\phi, m]$  is given in terms of the elliptic integral of the first kind by (31).

$$\mathbf{F}^*[\phi|m] = \int_{\theta=0}^{\theta=\phi} \frac{1}{\sqrt{1 - m \sin^2(\theta)}} d\theta \quad (31)$$

159 Equation (29) is valid for any observation point  $M(r, \theta, z)$  with  $0 \leq \theta \leq 2\pi$ . Figure 8 represents  
 160 the field axial component  $H_z(r, \theta, z)$  versus the radial distance  $r$  of the observation point. The parameter  
 161 values which are taken for the calculation are  $h = 3$  mm,  $\theta_1 = 0$  rad,  $\theta_2 = \frac{\pi}{2}$  rad,  $\theta = 0$  rad,  $r_{in} = 25$  mm,  
 162  $r_{out} = 28$  mm.

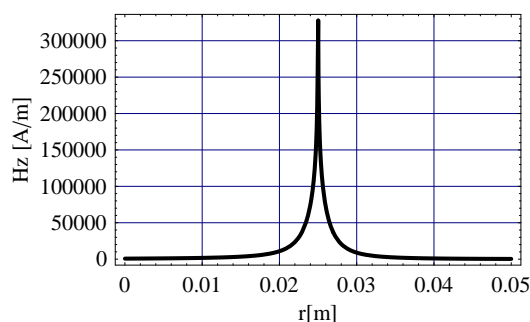


Fig. 8. Field axial component  $H_z(r, \theta, z)$  versus the radial distance  $r$  of the observation point;  $h = 3$  mm,  $r_{in} = 25$  mm,  $r_{out} = 28$  mm,  $\theta_1 = 0$  rad,  $\theta_2 = \frac{\pi}{2}$  rad,  $\theta = \frac{\pi}{2}$  rad

#### IV. CONCLUSION

This paper gives the analytical expressions of the three components of the magnetic field created by tile permanent magnets whose magnetization is either radial or axial. When the tiles are axially magnetized, the magnetic field can be calculated using these expressions at any point in space. For radially magnetized tiles, the expressions given correspond to the field created by thin tiles, whose inner and outer radii are not too different, and can be used at any point of the space as well. The magnetic field is directly calculated, without the help of the magnetic potentials. The utility of such analytical expressions for the three components of the magnetic field created by tile permanent magnets lies in the fact that the related calculations have a low computational cost, especially with regard to methods using finite elements or finite differences, and that they allow efficient parametric optimization studies of devices, which is very important for all applications.

The Mathematica files containing the analytical expressions used to calculate the three components of the magnetic field for axial and radial magnetizations are available online [33].

#### REFERENCES

- [1] B. Azzerboni and G. Saraceno, "Three-dimensional calculation of the magnetic field created by current-carrying massive disks," *IEEE Trans. Magn.*, vol. 34, no. 5, pp. 2601–2604, 1998.
- [2] K. Kim, E. Levi, Z. Zabar, and L. Birenbaum, "Restoring force between two noncoaxial circular coils," *IEEE Trans. Magn.*, vol. 32, no. 32, pp. 478–484, 1996.

- 181 [3] K. Kim, E. Levi, Z. Zabar, and L. Birenbaum, "Mutual inductance of noncoaxial circular coils with constant current density,"  
182 *IEEE Trans. Magn.*, vol. 33, no. 32, pp. 4303–4309, 1997.
- 183 [4] O. M. Kwon, C. Surussavadee, M. V. K. Chari, S. Salon, and K. S. Vasubramaniam, "Analysis of the far field of permanent  
184 magnet motors and effects of geometric asymmetries and unbalance in magnet design," *IEEE Trans. Magn.*, vol. 40, no. 3,  
185 pp. 435–442, 2004.
- 186 [5] J. P. Selvaggi, S. Salon, O. M. Kwon, and M. V. K. Chari, "Calculating the external magnetic field from permanent magnets  
187 in permanent-magnet motors - an alternative method," *IEEE Trans. Magn.*, vol. 40, no. 5, pp. 3278–3285, 2004.
- 188 [6] S. Babic and C. Akyel, "Improvement in the analytical calculation of the magnetic field produced by permanent magnet rings,"  
189 *Progress in Electromagnetics Research C*, vol. 5, pp. 71–82, 2008.
- 190 [7] S. Babic and C. Akyel, "An improvement in the calculation of the magnetic field for an arbitrary geometry coil with rectangular  
191 cross section," *International Journal of Numerical Modelling: Electronic Networks, Devices and Fields*, vol. 18, pp. 493–504,  
192 November 2005.
- 193 [8] S. Babic and C. Akyel, "Magnetic force calculation between thin coaxial circular coils in air," *IEEE Trans. Magn.*, vol. 44,  
194 no. 4, pp. 445–452, 2008.
- 195 [9] J. P. Selvaggi, S. Salon, O. M. Kwon, and M. V. K. Chari, "Computation of the three-dimensional magnetic field from solid  
196 permanent-magnet bipolar cylinders by employing toroidal harmonics," *IEEE Trans. Magn.*, vol. 43, no. 10, pp. 3833–3839,  
197 2007.
- 198 [10] J. Conway, "Inductance calculations for noncoaxial coils using bessel functions," *IEEE Trans. Magn.*, vol. 43, no. 3, pp. 1023–  
199 1034, 2007.
- 200 [11] J. Conway, "Noncoaxial inductance calculations without the vector potential for axisymmetric coils and planar coils," *IEEE*  
201 *Trans. Magn.*, vol. 44, no. 10, pp. 453–462, 2008.
- 202 [12] E. Perigo, R. Faria, and C. Motta, "General expressions for the magnetic flux density produced by axially magnetized toroidal  
203 permanent magnets," *IEEE Trans. Magn.*, vol. 43, no. 10, pp. 3826–3832, 2008.
- 204 [13] Y. Zhilichev, "Calculation of magnetic field of tubular permanent magnet assemblies in cylindrical bipolar coordinates," *IEEE*  
205 *Trans. Magn.*, vol. 43, no. 7, pp. 3189–3195, 2007.
- 206 [14] E. P. Furlani, S. Reznik, and A. Kroll, "A three-dimensional field solution for radially polarized cylinders," *IEEE Trans. Magn.*,  
207 vol. 31, no. 1, pp. 844–851, 1995.
- 208 [15] E. P. Furlani, "A two-dimensional analysis for the coupling of magnetic gears," *IEEE Trans. Magn.*, vol. 33, no. 3, pp. 2317–  
209 2321, 1997.
- 210 [16] E. P. Furlani, "Field analysis and optimization of ndfeb axial field permanent magnet motors," *IEEE Trans. Magn.*, vol. 33,  
211 no. 5, pp. 3883–3885, 1997.
- 212 [17] H. L. Rakotoarison, J. P. Yonnet, and B. Delinchant, "Using coulombian approach for modeling scalar potential and magnetic  
213 field of a permanent magnet with radial polarization," *IEEE Trans. Magn.*, vol. 43, no. 4, pp. 1261–1264, 2007.
- 214 [18] K. Halbach, "Design of permanent multiple magnets with oriented rec material," *Nucl. Inst. Meth.*, vol. 169, pp. 1–10, 1980.
- 215 [19] J. Bird and A. Lipo, "Characteristics of an electrodynamic wheel using a 2-d steady-state model," *IEEE Trans. Magn.*, vol. 43,  
216 no. 8, pp. 3396–3405, 2007.

- 217 [20] J. Hilton and S. McMurry, "Halbach cylinders with improved field homogeneity and tailored gradient fields," *IEEE Trans.*  
218 *Magn.*, vol. 43, no. 5, pp. 1898–1902, 2007.
- 219 [21] Z. Zhu, Z. Xia, and D. Howe, "Comparison of halbach magnetized brushless machines based on discrete magnet segments or  
220 a single ring magnet," *IEEE Trans. Magn.*, vol. 38, no. 9, pp. 2997–2999, 2002.
- 221 [22] M. Aydin, Z. Zhu, T. Lipo, and D. Howe, "Minimization of cogging torque in axial-flux permanent-magnet machines: design  
222 concepts," *IEEE Trans. Magn.*, vol. 43, no. 9, pp. 3614–3622, 2007.
- 223 [23] Y. Li, J. Zou, and Y. Lu, "Optimum design of magnet shape in permanent-magnet synchronous motors," *IEEE Trans. Magn.*,  
224 vol. 39, no. 11, pp. 3523–4205, 2003.
- 225 [24] V. Lemarquand, J. F. Charpentier, and G. Lemarquand, "Nonsinusoidal torque of permanent-magnet couplings," *IEEE Trans.*  
226 *Magn.*, vol. 35, no. 5, pp. 4200–4205, 1999.
- 227 [25] J. F. Charpentier and G. Lemarquand, "Calculation of ironless permanent magnet coupling using semi-numerical magnetic  
228 pole theory method," *COMPEL*, vol. 20, no. 1, pp. 72–89, 2001.
- 229 [26] C. Blache and G. Lemarquand, "High magnetic field gradients in flux confining permanent magnet structures," *Journal of*  
230 *Magnetism and Magnetic Materials*, vol. 104, pp. 1111–1112, 1992.
- 231 [27] G. Lemarquand, "Ironless loudspeakers," *IEEE Trans. Magn.*, vol. 43, no. 8, pp. 3371–3374, 2007.
- 232 [28] R. Ravaud, G. Lemarquand, V. Lemarquand, and C. Depollier, "Ironless loudspeakers with ferrofluid seals," *Archives of*  
233 *Acoustics*, vol. 33, no. 4, pp. 3–10, 2008.
- 234 [29] R. Ravaud, G. Lemarquand, V. Lemarquand, and C. Depollier, "The three exact components of the magnetic field created by  
235 a radially magnetized tile permanent magnet.," *Progress in Electromagnetics Research, PIER* 88, pp. 307–319, 2008.
- 236 [30] R. Ravaud, G. Lemarquand, V. Lemarquand, and C. Depollier, "Discussion about the analytical calculation of the magnetic  
237 field created by permanent magnets.," *Progress in Electromagnetics Research B*, vol. 11, pp. 281–297, 2009.
- 238 [31] R. Ravaud, G. Lemarquand, V. Lemarquand, and C. Depollier, "Magnetic field produced by a tile permanent magnet whose  
239 polarization is both uniform and tangential," *Progress in Electromagnetics Research B*, vol. 12, 2009.
- 240 [32] R. Ravaud, G. Lemarquand, V. Lemarquand, and C. Depollier, "Analytical calculation of the magnetic field created by  
241 permanent-magnet rings," *IEEE Trans. Magn.*, vol. 44, no. 8, pp. 1982–1989, 2008.
- 242 [33] <http://www.univ-lemans.fr/~glemar>.